JOURNAL OF PROPULSION AND POWER
Vol. 11, No. 5, September–October 1995

Solid Rocket Motor Grain Burnback Analysis Using Adaptive Grids

R. J. Hejl* and S. D. Heister†
Purdue University, West Lafayette, Indiana 47907

This article describes a solid rocket motor ballistics tool capable of calculating burning surface area progressions in either axisymmetric or two-dimensional grains using adaptive gridding techniques. The main advantages of this tool are its ease of use and generalized capabilities in handling spatially dependent burning rate information. The solution algorithm determines optimal locations for the number of grain surface points desired by utilizing weighting factors. Wall proximity, surface curvature, and spatial burning rate variations are considered in assigning the value of this weighting factor.

Nomenclature

a, b = constants in weighting function, Eq. (4)
F_i = local value of weighting function, Eq. (4)
k = constant in burning rate expression, Eq. (7)
n = burning rate exponent
P = chamber pressure
R = radial coordinate
R_c = radius of curvature of propellant surface
R_{case} = radial distance to case wall
r = propellant burning rate
s = natural coordinate measured parallel to local grain surface
W_i = local wall proximity distance
W_{limit} = minimum allowable W_i value, Eq. (4)
w = web distance
Z = axial coordinate

Introduction

IT is well known that the chamber pressure and thrust of a solid rocket motor are functions of the surface area of the propellant exposed to the chamber environment. For this reason, the calculation of the "grain burnback" is of primary importance to solid rocket ballisticians. High accuracy is required of this calculation since the integral of the surface area history is directly proportional to the total mass of propellant and, hence, the total impulse of the motor. It is not a trivial task to create a model capable of handling arbitrary grain designs since burning surfaces may be created or consumed as a result of the burnback process. In addition, variations in internal insulation thickness generally lead to variations in the radius to the motor case wall, even though the case itself is constant diameter.

Current interests in the field of internal ballistics are aimed at increasing the fidelity of burning rate information utilized in the models. The inclusion of strain-augmentation and propellant rheological effects[1–4] have provided a challenge for surface geometry models due to the increased spatial dependence of burning rate implied by these phenomena.

Presented as Paper 94-3330 at the AIAA/ASME/SAE/ASEE 30th Joint Propulsion Conference, Indianapolis, IN, June 27–29, 1994; received July 29, 1994; revision received Dec. 5, 1994; accepted for publication Feb. 7, 1995.

*Graduate Student, School of Aeronautics and Astronautics. Member AIAA.
†Associate Professor, School of Aeronautics and Astronautics. Member AIAA.

Early grain burnback models require a definition of the initial port geometry through the use of a series of bounding surfaces composed of cylinders, cones, prisms, or spheres.[5] This surface modeling methodology has been employed in the industry standard solid propellant rocket motor performance computer program (SPP).[6–9] The main advantage of this approach lies in the accuracy of the formulation, i.e., spherical surfaces are represented exactly by specifying the origin and radius of the sphere. However, this technique is less adaptable to surfaces of a general (nonconic section) shape and for problems involving spatial burning rate dependence. In addition, the definition of all the bounding surfaces required to model the grain can be quite tedious, especially for three-dimensional problems.

Additional ballistic codes developed through the years have also relied on a similar method of grain regression. Although each may have represented unique and viable methods, they were still unable to accurately incorporate spatial burning rate variations in the grain burnback. One of these models was by Sforzini.[10] His model used the direct pattern search optimization technique. Another model was developed by Shatz et al.[11] This code dynamically synthesized the grain by first determining the optimal deployment of nodes for the planar configuration and then constructed a spline satisfying both the minimum fillet radii and burning perimeter requirements.

More recently, advanced models using both finite element and finite volume approaches have been developed by solid rocket propulsion contractors in the U.S. It is difficult for outside organizations to gain detailed information regarding these models due to their proprietary nature. To obtain accurate surface area predictions using these techniques often requires large grids and considerable computational expense[12] since the location of the surface is interpolated based on predetermined nodal locations. In addition, it is difficult to provide the necessary grid refinement for curved surfaces that are formed during the surface evolution. Finally, these techniques require significant effort to construct an adequate grid for a given problem and have not considered spatially dependent burning rate information.

With these ideas in mind, we have developed an alternate approach to the surface modeling required for grain burnback analysis. The goal of this effort was to develop a state-of-the-art code that is capable of optimizing the distribution of grain points to account for wall proximity or regions of curvature that develop as a result of the initial port geometry or from spatial burning rate variations. Ease of use has also played a major role in the development of this model. This approach lends itself to be ideally suited for the analysis of complex grain designs or spatially dependent burn rates.

Technical Approach

The model that has been developed has the general capability to handle axisymmetric or two-dimensional grains, although the bulk of the development was conducted using axisymmetric simulations. Much effort was expended to minimize the number of inputs required to generate an acceptable solution. Conceptually, only initial port and motor case geometries are required for problems in which spatial burning rate variations are negligible. In addition to these data, we require a choice of the total number of nodes initially used to represent the inner port surface as well as the nominal web increment between successive solutions. In the case where burning rates vary with position, this functionality must be included (either in tabular or equation form), and the nominal web increment represents a nominal web distance moved over a single burnback interval.

In describing the model, we shall assume an axisymmetric geometry. All ideas presented are extendable to the two-dimensional geometry with an appropriate change in coordinates. For an axisymmetric problem the initial propellant grain boundary can be represented by a series of R, Z points. Along with the coordinates of a given point, the user will also need to identify the point location. The designators B, S, C, and W are used to distinguish points that lie along the bore, slots, corners, and at wall boundaries, respectively, as indicated in Fig. 1. In addition, an R_s point will represent the origin of a circular arc. An R_s point also requires the input radius value, and the designation as either concave (cv) or convex (cx) to the grain surface. These features simplify the initial bore geometry specifications.

The B designation permits the code to calculate applicable port areas corresponding to the radial location of these points. Points designated S can be used to determine the mass flow out of the slot for pressure drop and momentum balance calculations. Points lying at a corner (C) will require special treatment since they may be lost at an inward burning corner. Finally, motion of the W points can be used to analyze insulation exposure times for the particular grain geometry being considered and insure high accuracy during propellant sliver burnout at the end of the firing.

Weighting Function

The primary innovation incorporated in the present work is the development of a numerical mesh generator with the capability to dynamically redistribute the placement of points defining a given grain geometry as it burns back. Here, we take advantage of the fact that the surface area of a linear segment can be obtained exactly by the use of nodes only at the ends of the segment. Therefore, all excess nodes are automatically placed in regions of curvature. As regions of curvature appear (and disappear) throughout the burnback process, the nodes are continually reassigned to minimize errors in surface area.

The key to this process is based on the calculation of a weighting function for each point defining the grain surface. This function must be capable of representing the effects of surface curvature (arising from either grain design or spatially dependent burning rates) and a point's proximity to the case wall. To accomplish the first task, finite differencing techniques are used to determine the local radius of curvature.[13] By using a local radius of curvature to assign point spacing, points will be concentrated in regions of high curvature so that straight lines can be used to connect neighboring points. The wall proximity is governed by the difference between the inner case radius and the radius to the grain point. This can be expressed as

$$W_i = R_{\text{case}_i} - R_i \tag{1}$$

Since the points are distributed due to their proximity to the previous neighbor, a natural coordinate s is defined as being everywhere parallel to the surface:

$$s_i = \sum_{i=1}^{j} \sqrt{(R_i - R_{i-1})^2 + (Z_i - Z_{i-1})^2} \tag{2}$$

Thus, s increases monotonically along the length of the grain and provides a calculation of the surface length.

The local radius of curvature R_c is calculated using the parameterization in terms of s. For example, in the axisymmetric grain we have

$$R_c = \frac{[(R')^2 + (Z')^2]^{1.5}}{|R'Z'' - Z'R''|} \tag{3}$$

where the primes represent differentiation with respect to s. Centered differencing is used to evaluate the derivatives of Eq. (3) at all points except corners and walls. The derivatives for corners are calculated by taking the average of a forward and backward difference, whereas wall points use either a forward or backward difference.

In order to incorporate local curvature and wall proximity effects, a weighting function[14] is defined

$$F_i = \frac{a}{R_{c_i}} + \frac{b}{\max(W_i, W_{\text{limit}})} \tag{4}$$

where the constants a, b are selected to obtain the optimal weight representative of the grid distribution. As is evident from the equation, the smaller the radius of curvature or the closer to the wall, the larger the weight will be.

The first step in the application of this method is to obtain an average weight value F_{avg} for the grain prior to the point redistribution. The process utilized to accomplish this task was to first generate an equidistant grain (a grain having an approximately equal spacing of points around the grain surface, also referred to as the "base case" shown in Fig. 2).

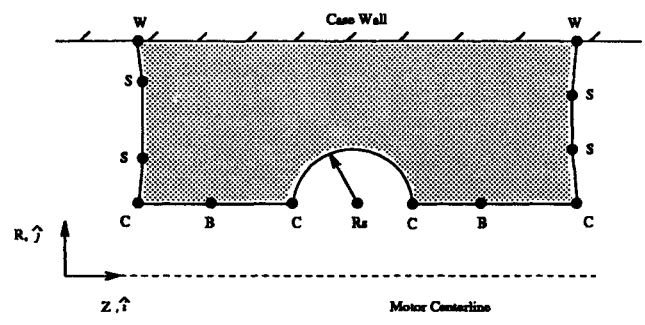

Fig. 1 Definition of "C, B, S," and "W" nodal designations.

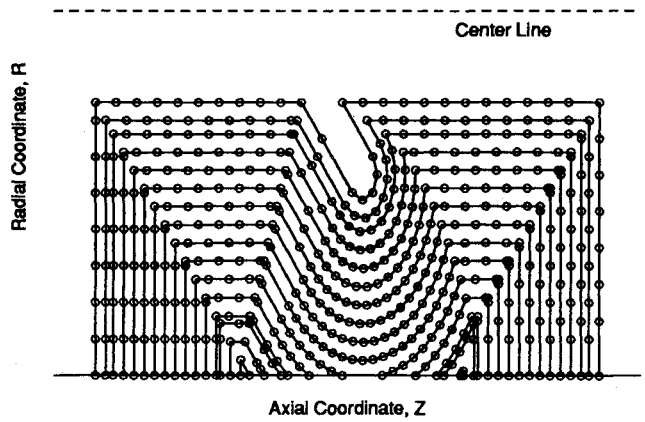

Fig. 2 Example base case for simple axisymmetric slotted grain.

With the base case point distribution setup, the weight for each point is calculated, and knowing the total number of points in the grid the average is then calculated. Furthermore, it is also assumed that the calculated weight for the corner and wall points will not vary between the base case and actual grains. This allows these positions to maintain a fixed weight prior to the redistribution of the input grain. It should be noted that the total number of points used in the adaptive solution will either be equal to or less than the total number from the base case.

After the average weight is known, nodes can be redistributed along the grain. The next step in this process is the actual placement of new grid points based on locations of the corner, wall, and arc points in the base case. The corner and wall points obtained from the base case are held fixed during this process. The distance between points is determined by

$$\delta_s = F_{\text{avg}}/F_i \tag{5}$$

where δ_s is the displaced distance along s where the point should be placed, and F_i is the weight of the current position on the grain. Thus, if the weight of point i is greater than the average, it means this point is in a region of high curvature or near the wall, and will dictate that the next point be a fraction of the spacing distance away. If this spacing exceeds the distance to the next corner or wall node, we do not place any additional nodes on the segment connecting these two points. While Eq. (5) allows very large spacing between points (when $F_i << F_{\text{avg}}$), we have not observed any problems in spacing the points too close together for reasonable grain geometries. For this reason, there is no need to place a restriction on the minimum possible size of δ_s for practical grain geometries.

Selection of Constants in Weighting Function

The success of the adaptive gridding procedure lies in the determination of suitable constants a and b in order to minimize the error in the burn surface area calculation as compared to an exact solution. Since the weighting function was designed to allow the modeling of grains with spatially dependent burn rates, the development of curvature during burnback is of primary concern. Therefore, the first term a/R_c should be much larger than the second b/W, which implies the constant a should be much larger than b. Using this approach will permit regions of high curvature to be more accurately modeled by placing more points in these areas due to the increased value of the corresponding weight F_i.

At first it would appear that wall proximity is of little use in the analysis since the primary effect being modeled is the curvature. However, if the second term is removed and there is an initial arc present in the grain, all the redistributed points will generally be placed in the region of the arc. Since only two points are used to define flat surfaces, the code will no longer be able to model spatial burn rate variations. Therefore, the inclusion of the proximity term allows for the modeling of curvature that develops during the grain burnback. In addition, this term promotes accurate modeling of propellant slivers frequently formed in the latter stages of the burnback process.

The desire to allow for this wall proximity effect dictates that the combination of a and b must be chosen so that a is larger than b, but not so large that b has no effect. Numerous calculations on several test cases were performed to determine this balance. Figure 3 shows the general trend from this analysis, indicating that the error is decreased for increasing a and decreasing b. In this figure, the "Total Error" represents a summation of the average errors in burning surface area from each of seven test cases used in this study (many of which are shown in the next section).

Since the area is a monotonic summation of straight line segments, some error will always exist when calculating the

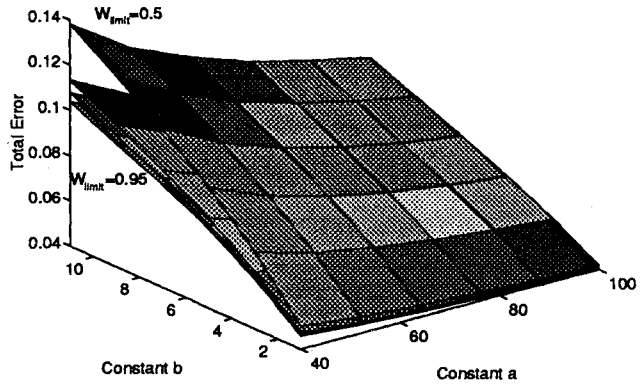

Fig. 3 Total error in burning surface area at various wall proximity limits.

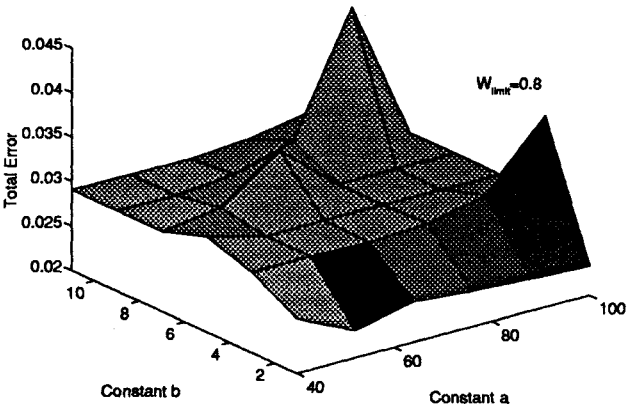

Fig. 4 Total error in burning surface area for wall proximity limit of $0.80\Delta w$.

area of an arc. With this in mind, it would initially appear that the ideal selection would be for a to equal the highest value allowable and b to equal the minimum value within the range considered. However, an additional feature of the weight calculation was to place a limit on the allowable minimum for the wall proximity of the grain. This minimum distance was set so that any points less than the limit would be assigned the minimum value. Since the wall proximity goes to zero as the radial component of the grain approaches the radial distance to the case, a minimum value W_{limit} is required so that the function F remains finite [see Eq. (4)].

The wall proximity limit must provide two things. First, it must ensure that the grain burning characteristics near the wall are properly modeled and it also must ensure that the wall points are not being overemphasized. Since these two ideas are somewhat contradictory, the limit must be a compromise between the two. Guided by these concerns, the value W_{limit} was selected accordingly.

Both b and W_{limit} must be set such that they combine to provide an accurate representation of the redistributed grid, while not overspecifying the side walls and inducing more errors in the area calculation. Using a range of constants and wall proximity limits, the optimum constant selection was obtained

$$a = 75, \quad b = 4, \quad W_{\text{limit}} = 0.80\Delta w \tag{6}$$

where Δw is the web increment input for the given calculation. In practice, Δw can also be estimated from the input time increment and average burning rate for a ballistics calculation. These values provide a reduction in average error while satisfying all of the requirements of grain modeling. Although $b = 1$ would provide lower errors, it does not allow proper regrid modeling along the end faces. This same reasoning was also used to eliminate larger values of a. Figure 4 shows an

additional error plot for a single test case consisting of spatially dependent burn rates (see Fig. 9 for geometry of this case). Using this grain model it was found that the value of $W_{\text{limit}} = 0.8\Delta w$ provided the largest reduction in error.

Results

The results from the model are compared with a base case in which the points are distributed in equal increments of arc length along a given segment of the grain. The base case serves not only as a means of comparison, but also provides initial values for the weighting function as described in the previous section. The total number of nodes in the base case calculation remains constant until propellant surfaces begin to hit the case wall or a surface burns out (which causes a decrease in the number of nodes). In all cases, the number of nodes in the adaptive grid is less than or equal to the number in the base case. It is natural to compare results with this base case since it represents a naive distribution of points.

The results obtained with the selected constants and wall proximity limit are presented in Figs. 5–8. Relatively simple geometries were considered in order that predicted surface areas could be compared to exact analytic calculations. The burning rate is assumed to have no spatial dependence in these calculations (to aid in simplifying the analytic solution). The error curves in these figures represent the difference between the two numerical approaches and the exact solution. These plots demonstrate the effect the weighting function has on the distribution of the grain points as compared to the base case. The maximum number of nodes ranges from 25 to 45 for these relatively simple examples.

Figure 5 demonstrates the results for a simple axisymmetric grain with an angled radial slot. It should be noted that the web increment is not constant for every step. As an intersection point for the grain is approached, the web increment is

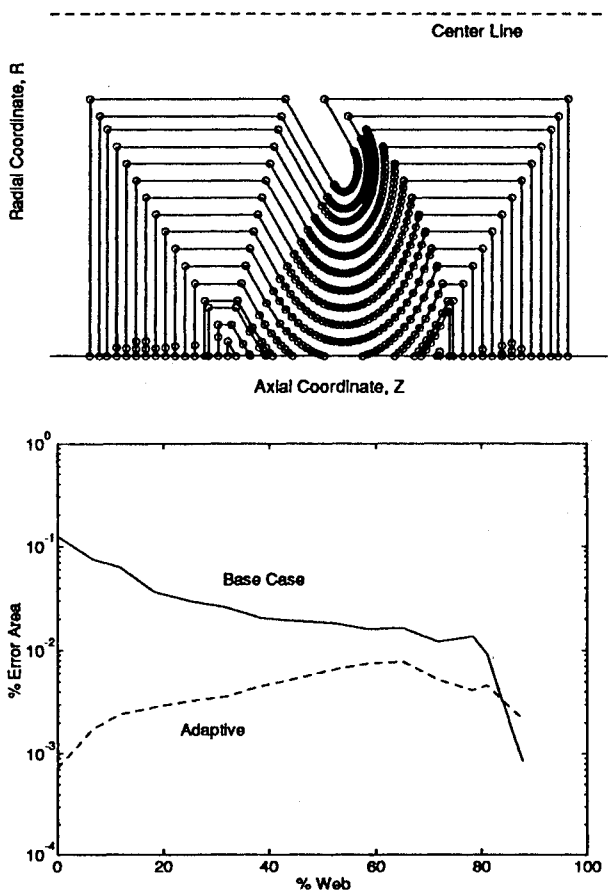

Fig. 5 Adaptive grain burnback and error prediction for grain with a radial slot.

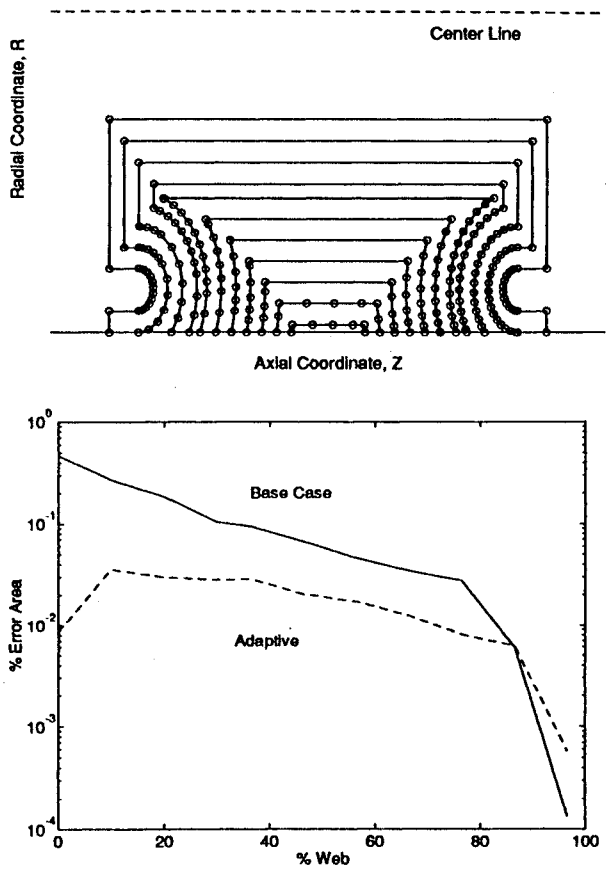

Fig. 6 Grain burnback and error prediction for axisymmetric grain with axial slots.

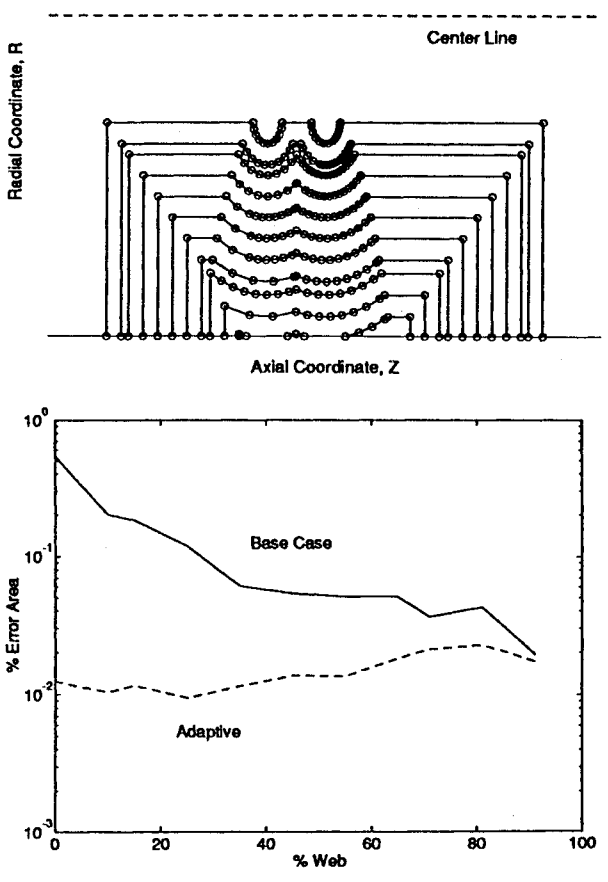

Fig. 7 Grain burnback and error prediction for axisymmetric grain with interacting radial slots.

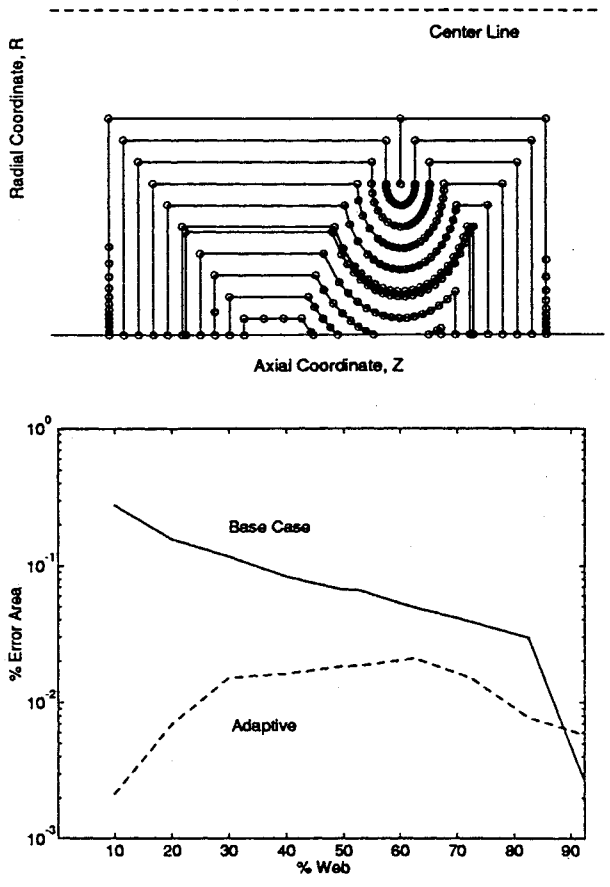

Fig. 8 Grain burnback and error prediction for an axisymmetric grain with a radial crack.

adjusted so that a solution is obtained exactly at the intersection point. While this type of adjustment is not necessary, it will improve the accuracy of the overall method. The adjustment is simple to make using the adaptive approach by monitoring proximity of all nodes with respect to a corner node.

Note the inclusion of a node near the wall in some of the burnbacks noted in Fig. 5. The adaptive procedure will place nodes in this location if the algorithm determines an adequate number of nodes is present along the arc. One can also note the effect of wall proximity on the node spacing of the arc as it approaches the wall. This feature assures accuracy in determining the areas of slivers which appear in this (and many other) grain designs.

The error plot in Fig. 5 notes the superiority of the adaptive grid over the naive point spacing utilized by the base case. Near burnout, the error in the adaptive grid may exceed that of the base case because surfaces of very small curvature are intersecting the case wall. The curvature may be small enough such that no points are placed along the arc. The optimal values for the constants a, b, and W_{limit}, were determined to reduce the average error at the expense of greater inaccuracy at the very end of the burnback process. Of course, greater accuracy can always be obtained by increasing the number of nodes.

Figure 6 is an example of a test grain designed to model the presence of stress-relief grooves along axial faces of a propellant segment. This grain design tests several aspects of the code, such as the formation of new wall points as an arc burns out and the intersection of a vertically oriented arc with a corner. Because the curvature of the arcs decreases as the grain burns back, the adaptive procedure reduces the number of nodes accordingly. Note that points appear on the horizontal surface as it approaches the wall due to the wall proximity influence included in the algorithm. The average error associated with the adaptive procedure is roughly an order of magnitude smaller than for the base case.

Figure 7 presents the grain burnback of two radial slots that interact and then burn out creating multiple surfaces along the wall. As the burnback approaches the wall, observe that the left slot has somewhat lower resolution. This phenomena is due to the point matching between the base and adaptive cases. As in all test cases, the number of nodes in the base case decreases as propellant is consumed. Since we have restricted the adaptive case to have no more points than the base, it was necessary for the code to remove the excess points. This feature can easily be modified to take full advantage of the adaptive method by simply allowing more points to be present during the latter stages of the burnback. We proceeded in the fashion described previously in order that the error comparison could be conducted in a rational fashion (with similar number of nodes for both cases). As in the other test cases, the adaptive procedure permits substantial reductions in error as compared to the base case.

Figure 8 illustrates the presence of an initial crack in the grain. The interesting point to note in this example is the initial distribution of points along the axial end faces of the grain. Since the input grain contained no regions of complex design, the weighting of the grain results in the placement of points along the end faces. As curvature develops as a result of the burnout of the crack, these points are distributed along the curved surface in order to improve accuracy. Note that the procedure always increments the web to the exact location of intersections of surfaces by monitoring the motion of corner nodes.

Application with Spatially Dependent Burning Rates

As mentioned in the Introduction, there is a growing body of evidence indicating that the inclusion of spatially dependent burning rate information can improve the fidelity of ballistic predictions. To verify the capabilities of the model in this situation, the model was compared against a recent analytic model developed by Heister.[4] This work presumed a standard burning rate pressure dependence as in St. Robert's law ($r \propto p^n$). The spatial burning rate dependence was introduced as a multiplicative factor

$$r = p^n(1 \pm k \sin\{\pi[(2w/w_m) - \tfrac{1}{2}]\}) \qquad (7)$$

where k is an amplification factor, and w and w_m are web distance and maximum (or total) web distance, respectively, as measured from the horizontal propellant surface shown in Fig. 9. Here, the upper sign is employed on axial faces, while the lower sign is used on surface defining the port. A sample case was run with a web fraction of 0.8, a max web of 4, a k value of 0.1, and a grain length of 16.

The result from the test case is shown in Fig. 9. Good agreement is obtained between the model predictions (of surface area) and the calculation via the analytic result even for this relatively coarse grid using 13 points. In this case, a significant error resulted in interpolating web increments from the analytic results for use in comparison with the model predictions.

Finally, note the incongruity in the number of points along the two axial-facing surfaces in some of the burnback locations. Similar behavior can also be noted in Figs. 5–8. This incongruity results from the fact that the algorithm restricts the number of nodes to be less than or equal to that of the base case. This restriction (which is incorporated for error comparisons only), occasionally requires that nodes be removed. The algorithm removes the nodes with the lowest F_i values, starting at the left end of the domain. In actual computations, this feature can easily be eliminated since the number of nodes at successive burnbacks is not a real issue. In

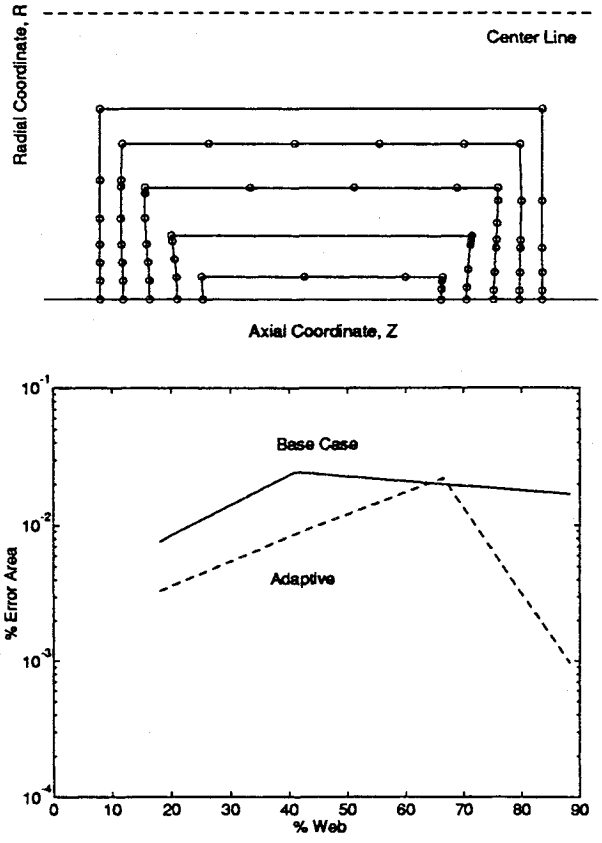

Fig. 9 Grain burnback and error prediction for a grain with spatially dependent burning rates.

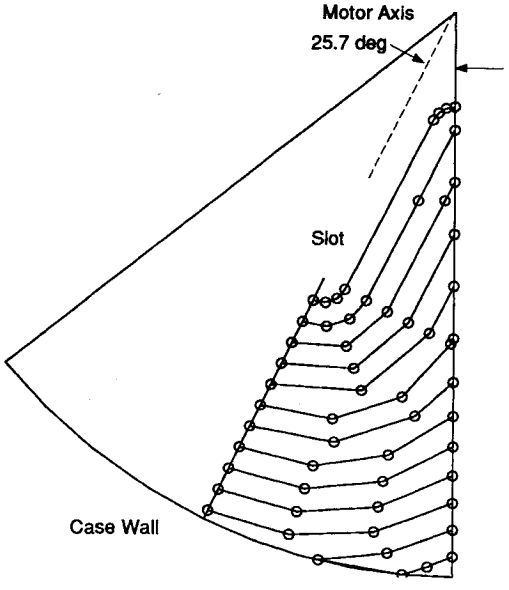

Fig. 10 Sample calculation for a two-dimensional grain with a seven-point star.

summary, the results indicate the capability of the model to address arbitrary spatially dependent burning rates.

Application to Two-Dimensional Grain Design

A limited amount of work has been performed for two-dimensional grain geometries. While the code in its current form can perform burnback calculations in this case, further refinements are necessary since the two-dimensional geometry necessitates a change in the radius of curvature calculation. While we have made limited attempts to reoptimize these constants for the two-dimensional case, additional efforts (on several test-case geometries) would be required to fully validate the model for the two-dimensional case. In principle, there is no reason why the technique cannot be successfully implemented in two- and three-dimensional geometries.

A sample result obtained for a typical two-dimensional star grain is presented in Fig. 10. The geometry is modeled to closely resemble the Star 12 rocket motor manufactured by Thiokol Corporation.[15] One-half of a given star point region is modeled in taking advantage of the symmetry involved in this particular grain design. Performance similar to the axisymmetric cases is noted, with nodes being placed in regions of high curvature or close to the wall.

Conclusions

The model described previously represents a unique, user-friendly tool for use in the analysis of a solid rocket motor grain burnback. By adaptively regridding the grain, a reduction in the error of the burning surface area calculation is obtained, as compared to current techniques. Error reductions of a factor of 10 have been obtained as compared to the base case involving evenly distributed points along the surface of the grain. The model is sufficiently general to handle arbitrary spatially dependent burning rate data and requires a minimum of user inputs.

References

[1]Beckman, C. W., and Geisler, R. L., "Ballistic Anomaly Trends in Subscale Solid Rocket Motors," AIAA Paper 82-1092, July 1982.

[2]Neilson, A. R., and Miles, W. L., "Space Shuttle Solid Rocket Motor Reproducibility and the Apparent Influence of Propellant Processing Characteristics on Trace Shape," AIAA Paper 89-2310, July 1989.

[3]Kallmeyer, T. E., and Sayer, L. H., "Differences Between Actual and Predicted Pressure-Time Histories of Solid Rocket Motors," AIAA Paper 82-1094, June 1982.

[4]Heister, S. D., "Ballistics of Solid Rocket Motors with Spatial Burning Rate Variations," *Journal of Propulsion and Power*, Vol. 9, No. 4, 1993, pp. 649–651.

[5]Peterson, E. G., Nielsen, C. C., Johnson, W. C., and Cook, K. S., "Generalized Coordinate Grain Design and Internal Ballistics Evaluation Program," AIAA Paper 68-490, June 1968.

[6]Coats, D. E., Nickerson, G. R., Dang, A. L., and Dunn, S. S., "Solid Performance Program (SPP)," AIAA Paper 87-1701, June 1987.

[7]George, D., "Recent Advances in Solid Rocket Motor Performance Prediction Capability," AIAA Paper 81-0033, Jan. 1981.

[8]Lamberty, J. T., "A Report on the Grain Design and Internal Ballistic Module of the Improved Solids Performance Program," AIAA Paper 81-0034, Jan. 1981.

[9]"The Solid Propellant Rocket Motor Performance Prediction Computer Program (SPP), Version 6.0," Air Force Astronautics Lab., AFAL-TR-87-078, Dec. 1987.

[10]Sforzini, R. H., "An Automated Approach to Design of Solid Rockets Utilizing a Special Internal Ballistics Model," AIAA Paper 80-1135, June 1980.

[11]Shatz, N., Tambour, Y., and Timnat, Y., "Dynamic Synthesis of Internal Burning Solid Propellant Grains," AIAA Paper 87-1735, June 1987.

[12]Eager, M. A., personal communication, Aerojet Corp., Yellow Creek, MI, 1991.

[13]Anderson, D. A., Tannahill, J. C., and Pletcher, R. H., *Computational Fluid Mechanics and Heat Transfer*, McGraw–Hill, New York, 1984.

[14]Thompson, J. F., Warsi, Z. U., and Mastin, C. W., *Numerical Grid Generation Foundations and Applications*, North-Holland, New York, 1985.

[15]*Thiokol Corporation Space Motor Catalog*, Tactical Operations, Elkton Div., Elkton, MD, 1991.